

Research Paper

Comprehensive Study of Free Vibration of Rectangular Mindlin's Plates with Rotationally Constrained Edges Using Dynamic Timoshenko Trial Functions

Yogesh VERMA, Nabanita DATTA

Indian Institute of Technology
Kharagpur, India
e-mail: yogesh.nitkl@gmail.com

A comprehensive theoretical study of the free vibration of rotationally restrained rectangular uniform isotropic Mindlin's plate is presented. The plate mode shape is assumed to be a weighted combination of the product of the Timoshenko beam functions in the either direction, which are previously generated for rotationally constrained boundary conditions. The effect of the uniformly distributed rotational spring constant (modelling the edge) participates in the potential energy of the plate. The Rayleigh-Ritz method has been used to generate the natural frequencies and plate mode shapes for various intermediate boundary conditions, asymptoting to those of the plates with all possible (six) classical boundary conditions. Plates with various thickness ratios have been studied to converge the results to the corresponding Kirchhoff's frequencies. The eigenvectors from the eigenvalue problem have been scrutinized to establish the beam-wise modal participation from either direction into the final plate mode shape. The square Mindlin's plate mode shapes have been generated to establish the various types of frequencies; which have been innovatively named and categorized as the (i) single frequencies, (ii) repeated frequencies (identical twins) and (iii) non-repeated frequencies (fraternal twins). Plates with different rectangular aspect ratios have been also analysed to show the deviation in the frequencies and mode shapes from the square plate. Also, their asymptotic behaviour to the corresponding Timoshenko beam at extreme aspect ratios has been established.

Key words: Mindlin's plate; eigenvectors; plate mode shapes; Timoshenko beam function; elastically restrained edges; asymptotic study.

NOTATIONS

a, b, h – length, breadth and thickness of the plate [m],
 A – cross-sectional area [m²],
 A_S – aspect ratio of plate $A_S = b/a$ [-],
 D – plate rigidity [N · m],
 E, G – Young modulus, Shear modulus [N/m²],

- I – area moment of inertia of cross section [m^4],
- k^2 – shear correction factor for shear strain,
- k_r – rotational restraint at the edges [$\text{N} \cdot \text{m}/\text{rad}$],
- K_{RR}, K_{RL} – right and left non-dimensional rotational restraint on the beam [-],
- K_R, R – non-dimensional rotational restraint on the plate edge [-],
- \mathbf{K}, \mathbf{M} – stiffness matrix and mass matrix,
- L – length of the beam [m],
- x, y, t – independent variable in length, breadth and time [m], [m], [s],
- U, T – strain energy and kinetic energy [J],
- $w(x, y; t)$ – lateral displacement [m],
- $W(x, y)$ – lateral out of plane displacement of the plate [m],
- W_{xi}, W_{yj} – beam mode shape in x and y -direction [m],
- ρ, ν – density of the material, Poisson ratio [kg/m^3],
- ξ, η – non-dimensional length, breadth of the beam/plate [-],
- ω, Ω – non-dimensional and dimensional natural frequencies [-], [rad/s],
- $\Psi_x(\xi, \eta)$ – pure bending slope of plate in x -direction [-],
- Ψ_{xi}, Ψ_{xj} – pure bending slope mode shape of beam in x -direction [-],
- $\Psi_y(\xi, \eta)$ – pure bending slope of plate in y -direction [-],
- Ψ_{yi}, Ψ_{yj} – pure bending slope mode shape of beam in y -direction [-].

1. INTRODUCTION

Plates find a wide range of applications in mechanical, civil, aerospace, naval, and nuclear engineering. They have various boundary conditions, slenderness ratios, aspect ratios, and natural frequencies. Their static and dynamic analyses are both required for sound structural designs. The Kirchhoff's (classical) plate theory, which assumes 'pure bending', begins to fail for (i) higher thickness ratios ($h/b > 1/20$), when the shear deformation and rotary inertia become important, and for (ii) higher order frequencies of thin plates itself, when the wave number is high, causing appreciable shear deformation. This necessitates the application of the Mindlin's plate theory [17, 18], which includes the shear deformation and the rotary inertia of the plate. The former augments the potential energy of the plate, while the latter augments the kinetic energy. Their prominence is a function of the slenderness of the plate, and the overtone of the frequency. The governing differential equations comprise of the three coupled equations for the flexural displacement, and the two pure bending slopes in each direction.

Classical boundary conditions are nearly impossible to achieve in practical engineering applications, e.g. the quality of the weld on the edge of a plate maybe weak enough not to match with the classical 'clamped' condition. Even hinged edges need not be exactly 'classical' since some restraint is often provided for safety and operational ease. This necessitates the analysis of such plates using the special boundary conditions, which are modelled as rotational springs,

participating in the total potential energy of the plate. The natural frequency of the plate is highly sensitive to the (i) boundary conditions, (ii) slenderness ratio, and (iii) aspect ratio of the plate. Modelling of the boundary conditions of the plate through those of the admissible beam functions is still open to scrutiny, in at least vibration analysis. Thus, the objective of this work is as follows:

- The indirect modelling of the Mindlin's plate boundary condition through the Timoshenko beam boundary conditions, augmented by dummy rotational spring constants in the potential energy of the edge fixity: this eliminates the requirement of the dummy inclusion of translational constants to achieve the non-classical edge conditions of the plate, which is usually included in published work. This reduces the computational time of free vibration greatly.
- The study of plate mode shapes through eigenvectors, which is not yet found in the existing literature, which is limited to the frequency analysis only.
- The study of the asymptotic behaviour of the plate frequencies as a function of the aspect ratio, which is still unreported in published work.

MAGRAB [16] studied orthotropic rectangular Mindlin's plates with the edges modelled as torsional springs. The results were limited to the square plates only. DAWE and ROUFAEIL [5] investigated the Mindlin's plates for free vibration analysis by using Timoshenko beam functions as the admissible functions for the plate in the energy-based method, but for a limited number of classical boundary conditions only (6 out of 21). WARBURTON and EDNEY [22] investigated the free vibration of thin rectangular Kirchhoff's plates by using the Rayleigh-Ritz method, with the edges constrained both against translation and rotation. Similarly, LAURA [11, 10] and LAURA and GROSSI [10] worked with rectangular plates with edges elastically restrained against rotation, applying the Rayleigh-Ritz method. GORMAN [7, 8] and BAPAT [1] studied the free vibration analysis of rectangular and square plates, with all edges elastically supported, by using the superposition and Levy's method respectively. Results by GORMAN [7] are limited to the square plates only. BAPAT's work [1] was limited to Kirchhoff's plate. CHUNG *et al.* [2] studied the square Mindlin's plate analysis, with edges elastically restrained against rotation, by using 'static' Timoshenko beam functions as the admissible functions, which were generated by a 3rd degree polynomial. 'Static' stands for the ignoring of both translational inertia and rotary inertia of the beam. SAHA *et al.* [19] used the dynamic Timoshenko beam mode shapes as trial functions for the rectangular Mindlin plates with edges elastically restrained against both translation and rotation. XIANG *et al.* [23] studied Mindlin's plates with both translational and rotational edge constraints, by using complete 2-dimensional polynomial. Here, the trial func-

tions were directly for the plate, using a 14-degree polynomial to achieve high accuracy in satisfying the boundary conditions. ZHOU [24] studied moderately thick plates ($h/b = 0.2$) with both translational and rotational edge constraints, once again using the 'static' Timoshenko beam function as a trial function for rectangular Mindlin's plates. DE ROSA and LIPPIELLO [6] studied the free vibration of tapered Euler-Bernoulli beam with rotationally and axially elastically constraints. The cell discretization method (CDM) is used for dynamic analysis.

As per the knowledge of the authors, very few attempts have been made to investigate Mindlin's plates, with edges elastically restrained against rotation, using *dynamic Timoshenko beam* mode shapes; for a wide range of (i) non-dimensional rotational spring constants ($1-10^5$) and (ii) aspect ratios (0.1-10), over all possible permutations and combinations of edge constraints, leading to all possible six classical plates (SSSS, SSSC, SSCC, SCSC, SCCC, CCCC). For the first time, all six combinations of clamped and hinged sides have been analysed to generate convergent frequencies using only torsional springs (no translational springs). This has been made possible by using the correct dummy variables for the end fixities in the potential energy of the plate, bypassing the accurate formulation of the Mindlin's plate boundary conditions. Dynamic Timoshenko beam functions (from beam vibration analysis) have been employed as the trial/elementary/admissible functions into the Mindlin's plate, by using the energy-based Rayleigh-Ritz method (RRM). This work theoretically analyses the Mindlin's plates over a wide range of rotational edge constraints on one or more sides, for rectangular plates with different aspect ratios.

Here, as an innovative attempt, a further study of the Mindlin's plate mode shapes with respect to the individual eigenvectors, highlighting the modal participation from the two directions, has been done. A vast study of uniform, homogenous, isotropic, rectangular plates; with edges elastically restrained against rotation; for different slenderness ratios and aspect ratios, has been conducted. For the first time, the asymptotic behaviour of the plates with respect to the aspect ratio, over various boundary conditions, and two different thickness ratios have been clearly established. The structure of the paper is as follows:

- The problem statement has been defined with respect to the parametric space.
- Timoshenko beam vibration analysis has been discussed, which generates the admissible functions.
- Mindlin's plate analysis, by the energy-based RRM, has been detailed.
- Results for the square plate have been tabulated and discussed over the parametric space, including convergence and comparative studies.
- Square plate mode shapes for the six possible boundary conditions, along with their eigenvectors, have been scrutinized.

- Results for the rectangular plate have been tabulated and discussed over the parametric space, for two different aspect ratios, including convergence and comparative studies.
- The asymptotic behaviour of the rectangular plates has been done for various boundary conditions.

2. PROBLEM FORMULATION AND PARAMETRIC SPACE

A homogenous, isotropic and uniform rectangular Mindlin’s plate has been studied for free vibration natural frequencies and corresponding mode shape. The free vibration is analysed by the Mindlin’s plate theory which includes shear deformation and rotary inertia. The length of the plate is L [m], width B [m], thickness h [m], density of the material ρ [kg/m³], modulus of elasticity E [N/m²], shear modulus G [N/m²], Poisson ratio ν . The edge condition is considered to be special, modelled as a uniformly distributed torsional spring over the edge, with a spring constant of K_R [N · m/rad]. The study requires the analysis of the Timoshenko beam with rotationally constrained edges (Fig. 1), whose closed-form dynamic mode shapes are input into the RRM to analyse the Mindlin’s plate with uniformly distributed rotationally constrained edges (Fig. 2). This work encompasses the following parameters:

- *Boundary conditions:* All possible permutations and combinations of simply supported and clamped edges have been used here, by adjusting the torsional spring constant of the edge(s), leading to the six classical plates; namely, SSSS, CCCC, CCSS, SCSS, CCCS, SCSC.
- *Edge constraint:* The influence of the rotational constraint of the edges on the plate natural frequency is studied over a wide range; starting from the SSSS plate, and approaching to the five plates above.
- *Slenderness ratio:* Increasing the thickness-to-length ratio increases the prominence of shear deformation, especially at the higher modes. In this

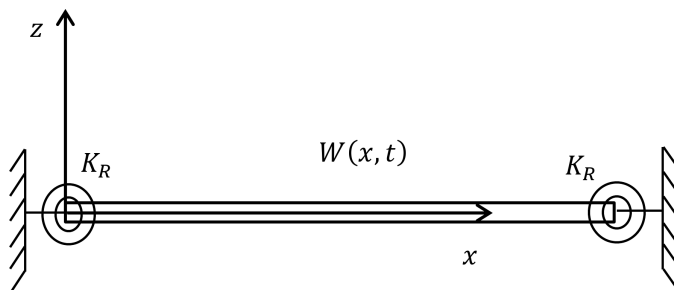


FIG. 1. Timoshenko beam with rotationally restrained edges.

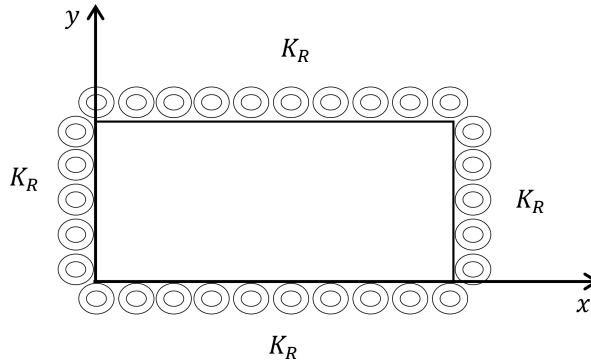


FIG. 2. Mindlin's plate with rotational edge constraints.

work, three different slenderness ratios have been studied: $h/b = 0.001$ (for convergence with Kirchhoff's plate), $h/b = 0.01$ and $h/b = 0.1$.

- *Aspect ratio*: All the above plates have been studied for four different aspect ratios, i.e. $a/b = 1$ (for convergence to Kirchhoff's plate), $a/b = 0.4, 0.6, 1.0, 1.5$. The reciprocal aspect ratios produce the same natural frequencies and mode shapes, but only for the CCCC, SSSS, and CCSS plates.

3. ANALYSIS METHODOLOGY

The free vibration analysis of the Mindlin's plate is done by the energy-based RRM. This requires the generation of the orthogonal Timoshenko beam mode shapes, which are used as trial functions for the Mindlin's Plate.

3.1. Timoshenko beam vibration: trial function generation

The dynamic Timoshenko beam mode shapes derived from its free vibration analysis, have been used as the trial functions (admissible functions) in the energy based plate vibration analysis. The coupled system of governing differential equations, for the free vibration of Timoshenko beam [20], is given as:

$$(3.1) \quad \begin{aligned} EI \frac{\partial^2 \varphi(x, t)}{\partial x^2} + k^2 AG \left(\frac{\partial w(x, t)}{\partial x} - \varphi(x, t) \right) - I \rho \frac{\partial^2 \varphi(x, t)}{\partial t^2} &= 0, \\ \rho A \frac{\partial^2 w(x, t)}{\partial t^2} - k^2 AG \left(\frac{\partial^2 w(x, t)}{\partial x^2} - \frac{\partial \varphi(x, t)}{\partial x} \right) &= 0, \end{aligned}$$

where $w(x, t)$ is a lateral displacement, $\varphi(x, t)$ is a pure bending slope, A is the cross-sectional area, I is the second moment of area of the cross-section

about the neutral axis, and k^2 is the shear correction factor uniformly varying along the cross-section. The x -direction is along the length of the beam. Eliminating the pure bending slope $\varphi(x, t)$ from Eq. (3.1), the unified equation becomes [9, 21]

$$(3.2) \quad EI \frac{\partial^4 w}{\partial x^4} + \rho A \frac{\partial^2 w}{\partial t^2} - \rho I \left(1 + \frac{E}{k^2 G} \right) \frac{\partial^4 w}{\partial x^2 \partial t^2} + \frac{\rho^2 I}{k^2 G} \frac{\partial^4 w}{\partial t^4} = 0.$$

Similarly, eliminating the total displacement $w(x, t)$ from Eq. (3.1) we arrive at

$$(3.3) \quad EI \frac{\partial^4 \varphi}{\partial x^4} + \rho A \frac{\partial^2 \varphi}{\partial t^2} - \rho I \left(1 + \frac{E}{k^2 G} \right) \frac{\partial^4 \varphi}{\partial x^2 \partial t^2} + \frac{\rho^2 I}{k^2 G} \frac{\partial^4 \varphi}{\partial t^4} = 0.$$

Assuming the vibration to be harmonic in time, the dependent variables in Eq. (3.1) are expressed as: $w(x, t) = W(\xi) e^{i\Omega t}$, $\varphi(x, t) = \psi(\xi) e^{i\Omega t}$, $\xi = \frac{x}{L}$, where $W(\xi)$ is the Timoshenko beam mode shape and $\psi(\xi)$ is its pure-bending slope mode shape. The difference between $w'(x)$ and $\psi(x)$ is the shear slope (shear strain). The axis-system is located at one corner of the plate. The x -direction is along the length of the plate, and y -direction along the width. The spatial component becomes, from Eq. (3.2)

$$(3.4) \quad \frac{\partial^4 W(\xi)}{\partial \xi^4} + \Omega^2 \left(\frac{\rho L^2}{E} + \frac{\rho L^2}{k^2 G} \right) \frac{\partial^2 W(\xi)}{\partial \xi^2} + \frac{\rho^2 L^4 \Omega^4}{E k^2 G} W(\xi) - \frac{\rho A L^4 \Omega^2}{EI} = 0,$$

where the symbols combine the geometric and material properties as:

$$\Omega^2 = b^2 \frac{EI}{\rho A L^4}, \quad q_2 = \frac{I}{A L^2}, \quad q_1 = \frac{EI}{k^2 A G L^2},$$

where b^2 is the non-dimensional frequency or the frequency parameter. Thus,

$$(3.5) \quad W^{IV} + b^2 (q_1 + q_2) W'' - b^2 (1 - b^2 q_1 q_2) W = 0.$$

Similarly, Eq. (3.3) leads to

$$(3.6) \quad \psi^{IV} + b^2 (q_1 + q_2) \psi'' - b^2 (1 - b^2 q_1 q_2) \psi = 0.$$

Solving the bi-quadratic in Eq. (3.5), the solution can be expressed as:

$$\lambda^2 = \frac{-b^2 (q_1 + q_2) \pm \sqrt{b^4 (q_1 + q_2)^2 + 4b^2 (1 - b^2 q_1 q_2)}}{2},$$

$$\frac{\lambda}{b} = \left\{ \frac{-(q_1 + q_2) \pm \sqrt{(q_1 - q_2)^2 + \frac{4}{b^2}}}{2} \right\}^{1/2}.$$

Specifically,

$$\alpha = \frac{\lambda}{b} = \pm \left\{ \frac{-(q_1 + q_2) + \sqrt{(q_1 - q_2)^2 + \frac{4}{b^2}}}{2} \right\}^{1/2}$$

and

$$\beta = \frac{\lambda}{b} = \pm \left\{ \frac{-(q_1 + q_2) - \sqrt{(q_1 - q_2)^2 + \frac{4}{b^2}}}{2} \right\}^{1/2}$$

are the hyperbolic/monotonous part and the imaginary/oscillatory part, respectively. Thus, the general solution to Eq. (3.5) and Eq. (3.6) are, respectively, expressed as:

- Beam mode shape:

$$(3.7) \quad W(\xi) = C_1 \cosh \alpha b \xi + C_2 \sinh \alpha b \xi + C_3 \cos \beta b \xi + C_4 \sin \beta b \xi;$$

- Pure slope mode shape:

$$(3.8) \quad \psi(\xi) = \overline{C}_1 \cosh \alpha b \xi + \overline{C}_2 \sinh \alpha b \xi + \overline{C}_3 \cos \beta b \xi + \overline{C}_4 \sin \beta b \xi.$$

For $-(q_1 + q_2) > \left\{ (q_1 - q_2)^2 + \frac{4}{b^2} \right\}^{1/2}$; i.e. $\frac{1}{b^2} < q_1 q_2$, the parameter α will be hyperbolic in nature. Substituting for q_1, q_2, b^2 in Eq. (3.1)₁ gives:

$$(3.9) \quad q_1 \psi'' - (1 - q_1 q_2 b^2) \psi + \frac{W'}{L} = 0.$$

Similarly, substituting for q_1, q_2, b^2 in Eq. (3.1)₂ gives

$$(3.10) \quad W'' + b^2 q_1 W - \psi' L = 0.$$

Substituting for W, ψ and their first and second derivatives in Eq. (3.9) and (3.10), we arrive at four relationships among the coefficients of W, ψ as follows:

$$(3.11) \quad \begin{aligned} \overline{C}_1 &= \frac{b}{L} \frac{(\alpha^2 + q_1)}{\alpha} C_1, & \overline{C}_2 &= \frac{b}{L} \frac{(\alpha^2 + q_1)}{\alpha} C_2, \\ \overline{C}_3 &= -\frac{b}{L} \frac{[\beta^2 - q_1]}{\beta} C_3, & \overline{C}_4 &= \frac{b}{L} \frac{[\beta^2 - q_1]}{\beta} C_4. \end{aligned}$$

The coefficients of $W(\xi)$ and $\psi(\xi)$ depend on the boundary conditions of the beam. Here, the edges of the beam are elastically restrained against rotation, and the displacement is zero at the ends

$$K_1 = \frac{b}{L} \frac{(\alpha^2 + q_1)}{\alpha}, \quad K_2 = \frac{b}{L} \frac{(\beta^2 - q_1)}{\beta},$$

$$\lambda = \frac{\alpha}{\beta}, \quad \gamma = \frac{(\beta^2 - q_1)}{(\alpha^2 + q_1)}, \quad \frac{K_2}{K_1} = \gamma\lambda.$$

The total deflection is zero at the ends: this is a classical geometric boundary condition. The bending moment at the ends balances the torque stored in the torsional spring. The special boundary condition involves only the pure bending slope of the Timoshenko beam. The four boundary conditions can be mathematically expressed as:

$$(3.12) \quad \begin{aligned} W(0) &= 0, & \psi(0) &= \frac{1}{K_{RL}}\psi'(0), \\ W(1) &= 0, & \psi(1) &= -\frac{1}{K_{RR}}\psi'(1), \end{aligned}$$

where K_{RR} and K_{RL} are the right and left side spring constants divided by EI. Substituting Eq. (3.12) in Eq. (3.7) and (3.8);

$$(3.13) \quad \begin{aligned} 0 &= C_1 + C_3, \\ K_1 C_1 \alpha b - K_1 K_{RL} C_2 - K_2 \beta b C_3 - K_{RL} K_2 C_4 &= 0, \\ C_1 \cosh \alpha b + C_2 \sinh \alpha b + C_3 \cos \beta b + C_4 \sin b\beta &= 0, \\ [K_{RR} \sinh \alpha b + \alpha b \cosh \alpha b] C_1 + [K_{RR} \cosh \alpha b + \alpha b \sinh \alpha b] C_2 \\ &+ [-K_{RR} \gamma \lambda \sin b\beta - \lambda \gamma \beta b \cos b\beta] C_3 \\ &+ [K_{RR} \gamma \lambda \cos b\beta - \gamma \lambda \beta b \sin b\beta] C_4 = 0. \end{aligned}$$

Writing Eq. (3.13) in the matrix form:

$$\begin{vmatrix} d_{11} & d_{12} & d_{13} & d_{14} \\ d_{21} & d_{22} & d_{23} & d_{24} \\ d_{31} & d_{32} & d_{33} & d_{34} \\ d_{41} & d_{42} & d_{43} & d_{44} \end{vmatrix} \begin{pmatrix} C_1 \\ C_2 \\ C_3 \\ C_4 \end{pmatrix} = \begin{pmatrix} 0 \\ 0 \\ 0 \\ 0 \end{pmatrix},$$

where $d_{11} = 1, d_{21} = \alpha b, d_{12} = 0, d_{22} = -K_{RL}, d_{13} = 1, d_{23} = -\gamma \lambda \beta b, d_{14} = 0, d_{24} = -K_{RL} \gamma \lambda, d_{31} = \cosh \alpha b, d_{41} = K_{RR} \sinh \alpha b + \alpha b \cosh \alpha b, d_{32} = \sinh \alpha b, d_{42} = K_{RR} \cosh \alpha b + \alpha b \sinh \alpha b, d_{33} = \cos \beta b, d_{43} = -K_{RR} \gamma \lambda \sin b\beta - \lambda \gamma \beta b \cos b\beta, d_{34} = \sin b\beta, d_{44} = K_{RR} \gamma \lambda \cos b\beta - \gamma \lambda \beta b \sin b\beta.$

For a non-trivial solution of the system of Eqs. (3.13),

$$(3.14) \quad \begin{vmatrix} d_{11} & d_{12} & d_{13} & d_{14} \\ d_{21} & d_{22} & d_{23} & d_{24} \\ d_{31} & d_{32} & d_{33} & d_{34} \\ d_{41} & d_{42} & d_{43} & d_{44} \end{vmatrix} = 0$$

gives the frequency equation. From here, the parameter b is obtained, which leads to the natural frequencies of the Timoshenko beam. Substituting for b in Eqs. (3.7) and (3.8), the Timoshenko beam mode shape and its pure-bending-slope mode shape are both generated. The mode shapes depend on the boundary conditions, which are governed by the non-dimensional torsional spring constant K_R . In this work, a wide range of K_R has been used to study the free vibration of the Mindlin's plate. The two extreme cases of the end fixity are as follows:

- for $K_R \geq 10^7$, the edge behaves like the classical clamped (built-in) edge,
- for $K_R \leq 10^{-7}$, the edge behaves like the classical hinged (simply-supported) edge.

3.2. Mindlin's plate vibration

Once the Timoshenko beam mode shapes are ready, they can be used as admissible/trial functions in the plate mode shape $W(\xi, \eta)$, and the pure bending slope mode shape $\Psi_x(\xi, \eta)$ and $\Psi_y(\xi, \eta)$. The independent variables are x [m] along the length, y [m] along the breadth and t in time [s]. The unknowns are, transverse out-of-plane flexural displacement $w(x, y; t)$, the pure bending slope along the x -direction $\Phi_x(x, y; t)$, the pure bending slope along the y -direction $\Phi_y(x, y; t)$. The three dependent variables/unknowns are expressed as:

$$\begin{aligned} w(x, y; t) &= W(\xi, \eta) e^{i\Omega t}, & \Phi_x(x, y; t) &= \Psi_x(\xi, \eta) e^{i\Omega t}/a, \\ \Phi_y(x, y; t) &= \Psi_y(\xi, \eta) e^{i\Omega t}/b, \\ \xi &= \frac{x}{a}, & \eta &= \frac{y}{b}, & q &= \frac{D}{k^2 G h a^2}, & A_s &= \frac{a}{b}, & t &= \frac{h}{b}. \end{aligned}$$

The curvature-coupled boundary conditions of the plate, after approximation (LAURA, GROSSI [10]) are:

- the total displacement is zero at the four edges
 $W(\xi, 0) = 0, \quad W(\xi, 1) = 0, \quad W(0, \eta) = 0, \quad W(1, \eta) = 0,$
- the bending moment at the edges is balanced by the torque stored in the torsional spring

$$\begin{aligned} K_{R1} \Psi_y(x) &= D \Psi'_y(x), & K_{R2} \Psi_x(y) &= D \Psi'_x(y), \\ K_{R3} \Psi_y(x) &= D \Psi'_y(x), & K_{R4} \Psi_x(y) &= D \Psi'_x(y). \end{aligned}$$

The maximum strain potential energy stored in a plate [17] is:

$$\begin{aligned}
 (3.15) \quad U_{\max(\text{plate})} = & \frac{1}{2} \frac{Db}{a^3} \int_0^1 \int_0^1 \left\{ \left(\frac{\partial \Psi_x}{\partial \xi} \right)^2 + A_s^4 \left(\frac{\partial \Psi_y}{\partial \eta} \right)^2 + 2A_s^2 \frac{\partial \Psi_x}{\partial \xi} \frac{\partial \Psi_y}{\partial \eta} \right. \\
 & - 2(1 - \nu) A_s^2 \left[\frac{\partial \Psi_x}{\partial \xi} \frac{\partial \Psi_y}{\partial \eta} - \frac{1}{4} \left(\frac{\partial \Psi_x}{\partial \eta} \right)^2 - \frac{1}{4} \left(\frac{\partial \Psi_y}{\partial \xi} \right)^2 \right] - \frac{1}{2} \frac{\partial \Psi_x}{\partial \eta} \frac{\partial \Psi_y}{\partial \xi} \\
 & \left. + \frac{1}{q} \left[\Psi_x^2 + \left(\frac{\partial W}{\partial \xi} \right)^2 + 2\Psi_x \frac{\partial W}{\partial \xi} + A_s^2 \left(\Psi_y^2 + \left(\frac{\partial W}{\partial \eta} \right)^2 + 2\Psi_y \left(\frac{\partial W}{\partial \eta} \right) \right) \right] \right\} d\xi d\eta.
 \end{aligned}$$

The maximum strain energy stored in the rotational springs on the four edges is:

$$\begin{aligned}
 (3.16) \quad U_{\max(\text{rotational spring})} = & \frac{1}{2} K_{R1} \int_0^1 [\Psi_x^2]_{\xi=0} d\eta + \frac{1}{2} K_{R2} \int_0^1 [\Psi_x^2]_{\xi=1} d\eta \\
 & + \frac{1}{2} K_{R3} A_s^4 \int_0^1 [\Psi_y^2]_{\eta=0} d\xi + \frac{1}{2} K_{R4} A_s^4 \int_0^1 [\Psi_y^2]_{\eta=1} d\xi,
 \end{aligned}$$

where $K_{R1} = \frac{k_{r1}a}{D}$, $K_{R2} = \frac{k_{r2}a}{D}$, $K_{R3} = \frac{k_{r3}b}{D}$, $K_{R4} = \frac{k_{r4}b}{D}$ (k_{r1} , k_{r2} are the dimensional spring constants).

The above four variables in Eq. (3.16) are ‘dummy variables’, which need to be included in order to match the physical boundary conditions of the plate. For a fully clamped side, K_R may be any number, and the plate analysis converges to a clamped plate irrespective of the dummy variable. However, ‘loosening’ the torsional spring to achieve the hinged condition requires the K_R to be fixed at a very small number. This is over and above the fact that the admissible function, i.e. the Timoshenko beam mode shape, already has the effect of the torsional spring in-built into it, through the closed-form solution to Eq. (3.1). Equations (3.7) and (3.8) contain the mode shapes, whose curvatures directly influence the potential energy. Though this may appear redundant since the beam mode shape considers the torsional spring constant; the plate analysis with edge conditions modelled as a torsional springs requires a judicious input of the dummy variables to mathematically achieve the physical fixities of the plate. The choice of the admissible function into the Rayleigh-Ritz method influences the prominence of the dummy variables, as the torsional spring constant goes on reducing from the clamped edge condition to the hinged condition. Published work shows the popularity of using ‘Static Timoshenko beam functions’ or polynomials satisfying a static deflection of the beam. The weaker the trial function, the less accurate is the curvature and the potential energy, and therefore,

the more elusive is the choice of the dummy variables. The use of the superior dynamic Timoshenko trial functions, already satisfying the intermediate boundary conditions, renders Eq. (3.16) of the Rayleigh-Ritz method less influential on the total potential energy of the plate. Equation (3.15) itself is able to capture the total potential energy of the plate. This methodology thus has been able to generate all the six classical plates combining the clamped and hinged edges, i.e. CCCC, SSSS, CSCS, CSSS, SCSS, and SSCC. The maximum kinetic energy of the plate is:

$$(3.17) \quad T_{\max(\text{plate})} = \frac{1}{2} \rho h \Omega^2 ab \int_0^1 \int_0^1 \left[W^2 + \frac{1}{12} t^2 \left(\frac{\Psi_x^2}{A_s^2} + \Psi_y^2 \right) \right] d\xi d\eta.$$

The three unknowns, expressed as a weighted superposition of the Timoshenko beam mode shapes, are:

$$W(\xi, \eta) = \sum_i^r \sum_j^r c_{ij} W_{xi}(\xi) W_{yj}(\eta), \quad \Psi_x(\xi, \eta) = \sum_i^r \sum_j^r d_{ij} \psi_{xi}(\xi) W_{yj}(\eta),$$

$$\Psi_y(\xi, \eta) = \sum_i^r \sum_j^r e_{ij} W_{xi}(\xi) \psi_{yj}(\eta),$$

where c_{ij} , d_{ij} , e_{ij} are the unknown weights in the Rayleigh-Ritz assumption. The minimization of the difference between the maximum strain potential energy and the kinetic energy of the plate with respect to the unknown coefficients leads an eigenvalue problem, the non-trivial solution of which gives natural frequencies of the plate. Thus, minimizing the energy w.r.t. the unknown coefficients as follows:

$$\left(\frac{\partial}{\partial c_{ij}} \right) (U_{\max(\text{plate})} + U_{\max(\text{rotational spring})} - T_{\max(\text{plate})}) = 0$$

$$\left(\frac{\partial}{\partial d_{ij}} \right) (U_{\max(\text{plate})} + U_{\max(\text{rotational spring})} - T_{\max(\text{plate})}) = 0 \quad i, j = 1, 2, 3, \dots, r$$

$$\left(\frac{\partial}{\partial e_{ij}} \right) (U_{\max(\text{plate})} + U_{\max(\text{rotational spring})} - T_{\max(\text{plate})}) = 0$$

leads to

$$(3.18) \quad ([K_{\text{plate}} + K_{\text{rotational spring}}] - \omega^2 [M_{\text{plate}}]) \begin{Bmatrix} c \\ d \\ e \end{Bmatrix} = 0,$$

where the non-dimensional frequency $\omega^2 = \frac{\rho h \Omega^2 b^4}{D}$; with the dimensional frequency Ω^2 ;

$$\mathbf{K}_{\text{plate}} = \begin{bmatrix} K_{cc} & K_{cd} & K_{ce} \\ K_{cd} & K_{dd} & K_{de} \\ K_{ce} & K_{de} & K_{ee} \end{bmatrix}_{3r \times 3r}, \quad \mathbf{K}_{\text{rotational spring}} = \begin{bmatrix} 0 & 0 & 0 \\ 0 & K_{dd} & 0 \\ 0 & 0 & K_{ee} \end{bmatrix}_{3r \times 3r},$$

$$\mathbf{M}_{\text{plate}} = \begin{bmatrix} M_{cc} & M_{cd} & M_{ce} \\ M_{cd} & M_{dd} & M_{de} \\ M_{ce} & M_{de} & M_{ee} \end{bmatrix}_{3r \times 3r},$$

where r is the number of modes in each direction of the Timoshenko beam function.

The components of the stiffness matrix are:

$$K_{cc} = \sum_i^r \sum_j^r \left[\frac{1}{q} \left(\int_0^1 \int_0^1 \frac{\partial W_{xi}}{\partial \xi} \frac{\partial W_{xj}}{\partial \xi} W_{yi} W_{yj} \, d\xi \, d\eta \right. \right. \\ \left. \left. + \left(A_s^2 \int_0^1 \int_0^1 \frac{\partial W_{yi}}{\partial \eta} \frac{\partial W_{yj}}{\partial \eta} W_{xi} W_{xj} \, d\xi \, d\eta \right) \right) \right],$$

$$K_{cd} = \sum_i^r \sum_j^r \frac{1}{q} \left[\int_0^1 \int_0^1 \left(\frac{\partial W_{xi}}{\partial \xi} \psi_{xj} W_{yi} W_{yj} \right) \, d\xi \, d\eta \right],$$

$$K_{ce} = \sum_i^r \sum_j^r \frac{1}{q} \left[A_s^2 \int_0^1 \int_0^1 \left(\psi_{yi} W_{xj} W_{xi} \frac{\partial W_{yj}}{\partial \eta} \right) \, d\xi \, d\eta \right],$$

$$K_{dd} = \sum_i^r \sum_j^r \left[\int_0^1 \int_0^1 \left(\frac{\partial \psi_{xi}}{\partial \xi} \frac{\partial \psi_{xj}}{\partial \xi} W_{yi} W_{yj} \right) \, d\xi \, d\eta \right. \\ \left. + \frac{(1-\nu)}{2} A_s^2 \int_0^1 \int_0^1 \left(\psi_{xi} \psi_{xj} \frac{\partial W_{yi}}{\partial \eta} \frac{\partial W_{yj}}{\partial \eta} \right) \, d\xi \, d\eta + \frac{1}{q} \int_0^1 \int_0^1 \left(\psi_{xi} \psi_{xj} W_{yi} W_{yj} \right) \, d\xi \, d\eta \right. \\ \left. + K_{R1} \int_0^1 \psi_{xi}(0) \psi_{xj}(0) \, d\eta + K_{R2} \int_0^1 \psi_{xi}(1) \psi_{xj}(1) \, d\eta \right],$$

$$\begin{aligned}
K_{de} &= \sum_i^r \sum_j^r \left[A_s^2 \left(\int_0^1 \int_0^1 \left(\frac{\partial \psi_{xi}}{\partial \xi} W_{xj} \frac{\partial \psi_{yi}}{\partial \eta} W_{yj} \right) d\xi d\eta \right. \right. \\
&\quad \left. \left. + \frac{(1-\nu)}{2} \int_0^1 \int_0^1 \left(\frac{\partial \psi_{xi}}{\partial \xi} W_{xj} \frac{\partial \psi_{yi}}{\partial \eta} W_{yj} \right) d\xi d\eta \right) \right], \\
K_{ee} &= \sum_i^r \sum_j^r \left[A_s^4 \int_0^1 \int_0^1 \left(W_{xi} W_{xj} \frac{\partial \psi_{yi}}{\partial \eta} \frac{\partial \psi_{yj}}{\partial \eta} \right) d\xi d\eta \right. \\
&\quad + \frac{(1-\nu)}{2} A_s^2 \int_0^1 \int_0^1 \left(\frac{\partial W_{xi}}{\partial \xi} \frac{\partial W_{xj}}{\partial \xi} \psi_{yi} \psi_{yj} \right) d\xi d\eta \\
&\quad + \frac{1}{q} A_s^2 \int_0^1 \int_0^1 (W_{xi} W_{xj} \psi_{yi} \psi_{yj}) d\xi d\eta \\
&\quad \left. + K_{R3} A_s^4 \int_0^1 (\psi_{yi}(0) \psi_{yj}(0)) d\xi + K_{R4} A_s^4 \int_0^1 (\psi_{yi}(1) \psi_{yj}(1)) d\xi \right].
\end{aligned}$$

The components of the mass matrix are:

$$\begin{aligned}
M_{cc} &= \sum_i^r \sum_j^r \left[\int_0^1 \int_0^1 (W_{xi} W_{xj} W_{yi} W_{yj}) d\xi d\eta \right], \\
M_{dd} &= \sum_i^r \sum_j^r \left[\frac{t^2}{12 A_s^2} \int_0^1 \int_0^1 (\psi_{xi} \psi_{xj} W_{yi} W_{yj}) d\xi d\eta \right], \\
M_{ee} &= \sum_i^r \sum_j^r \left[\frac{t^2}{12} \int_0^1 \int_0^1 (W_{xi} W_{xj} \psi_{yi} \psi_{yj}) d\xi d\eta \right], \\
M_{cd} &= M_{ce} = M_{de} = 0.
\end{aligned}$$

Equation (3.18) is an *eigenvalue problem*, which is solved to generate the natural frequencies (eigenvalues) and the plate mode shapes, which can be arrived at from the eigenvectors, which are the coefficients C_{ij} considering the number of modes as r , the eigen value problem generates r^2 natural frequencies, and their corresponding mode shapes. The eigenvectors are r^2 in number, and each having r^2 elements.

4. RESULTS

This section presents the results from the Mindlin’s plate analysis, compared with published work. It has been divided into the first sub-section on square plates, whose frequencies have been compared with established results. The square plate mode shapes and the eigenvectors have been analysed, scrutinized, and classified. The second sub-section deals with rectangular Mindlin’s plates, which are a fresh addition to the existing literature. The plates have been analysed by the energy-based RRM, generating the natural frequencies for various boundary conditions, two different thickness ratios, four different aspect ratios, and over a wide range of rotational edge constraints.

4.1. Timoshenko beam with rotational restraint: free vibration

Figure 3a shows the mode shapes of the Timoshenko beam with rotationally constrained edges, for a rotational spring constant of $K_R = 10^{-6}, 10^{-4}, 10^{-2}, 10^0, 10^1, 10^2, 10^4, 10^6$. Increasing the spring constant decreases the end slopes due to the reactional end moments being generated. It is noticed at for $K_R = 10$, the transition from the simply-supported beam to the clamped-clamped beam occurs. This is also reflected in Fig. 3b, which shows the pure-bending slope mode shapes of the Timoshenko beam. These mode shapes act as trial functions in the Mindlin’s plate analysis, along with their derivatives. The mode shapes are normalized to 1, before being used as trial functions.

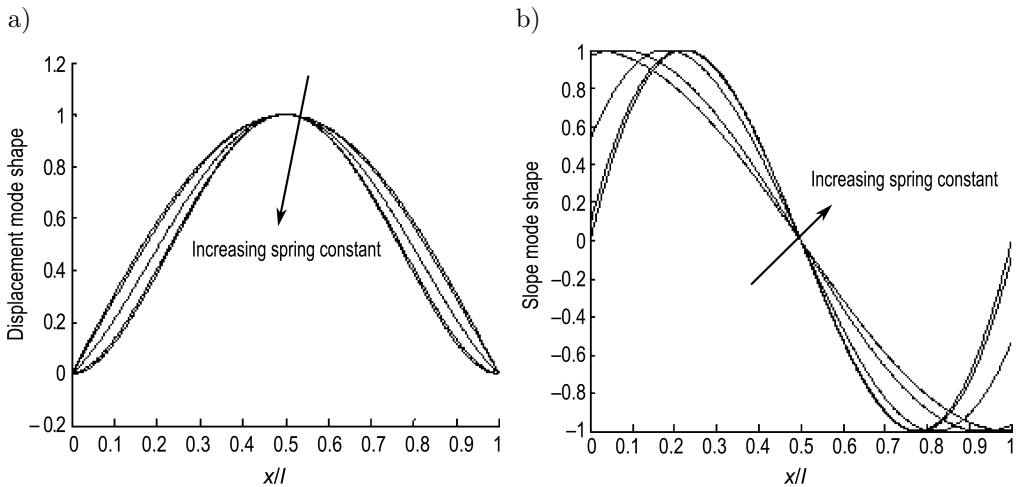


FIG. 3. Timoshenko mode shapes: a) deflection, b) pure bending slope for $K_R = 10^{-6}, 10^{-4}, 10^{-2}, 10^0, 10^1, 10^2, 10^4, 10^6$.

4.2. Square plate vibration

In this section, the free-vibration results for the uniform isotropic square Mindlin's plate are presented. Five different permutations/combinations of rotationally restrained boundary conditions have been analysed. Considering the plate to be a default SSSS plate (simply supported on all sides), the spring constant R is increased for one or more sides, to achieve the 5 different configurations below.

4.2.1. Non-classical edge conditions: parametric study. Figure 4 shows the first four frequency parameters of square plates, with two thickness ratios (0.01 and 0.1) and various boundary conditions, over a wide range of rotational spring constants of the edge constraint. Among the two thicknesses, the thicker plate yields a lower non-dimensional natural frequency; consistently for all the five plates. As the thickness increases, the shear deformation and rotary inertia both increase. In a Kirchhoff's plate, the potential energy is proportional to the cube of the plate thickness, but the kinetic energy is linearly proportional to thickness. However, in a Mindlin's plate, the inclusion of the rotary inertia causes the kinetic energy to become proportional to the cube of the thickness. Thus, the increase in kinetic energy overrides the increase in potential energy the increase in thickness of the plate, leading to a net decrease in the natural frequency. This trend is consistently seen in Fig. 4.

In Fig. 4a, the square plate has all edges equally constrained against rotation (denoted by R). As the spring constant increases, the frequency of the RRRR plate rises from the simply-supported plate behaviour to the clamped plate behaviour, with the transition zone between $10^0 < R < 10^3$, beyond which the spring constant can be safely assumed to replicate the classical clamped condition. Increasing the thickness of the plate leads to a decrease in the frequency parameter, which becomes more pronounced for the higher-order frequencies. Interestingly, this case precipitates a pair of repeated frequencies (ω_2 and ω_3), which overlap in the figure, for both the thicknesses and for all spring constants. This result has been consistently verified with SAHA *et al.* [19]. Figure 4c shows a similar behaviour for RRSS plate.

Figure 4b,d,e show the frequency parameters for RRRS, SRSR, and SSSR, respectively. As the limiting value of spring constant is increased from $1 < R < 5$ of the transition zone, the ω_2 and ω_3 overlap (SSSS behaviour); but as the spring constant further increases in $5 < R < 10^3$, ω_2 and ω_3 bifurcate apart from each other due to the increased beam-wise curvatures; for both thickness ratios, beyond which the spring constant is sufficient to replicate the clamped behaviour. Increasing the thickness of the plate leads to the shear deformation and rotary inertia becoming more prominent.

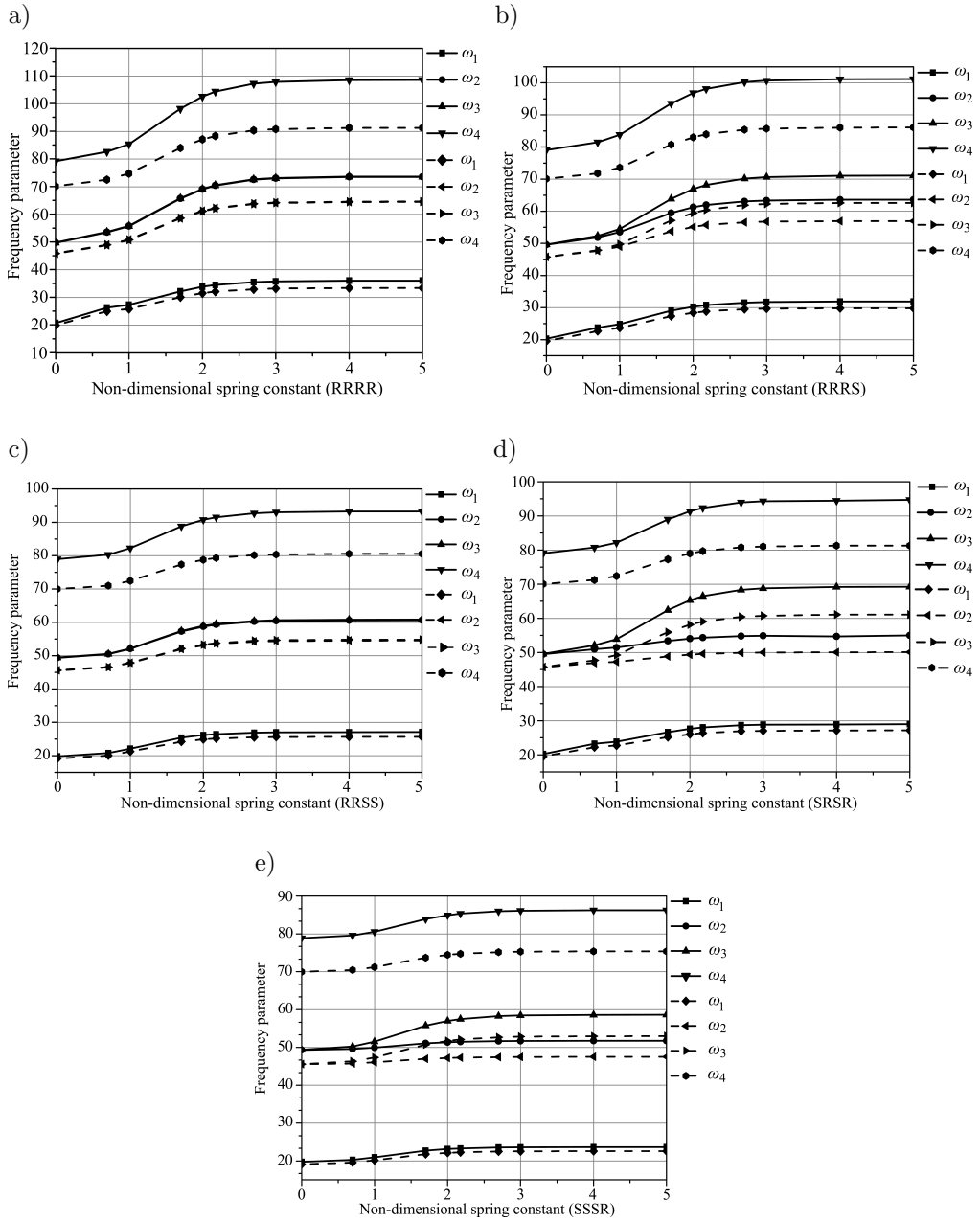


FIG. 4. First four natural frequencies of square Mindlin's plate: a) RRRR, b) RRRS, c) RRSS, d) SRSR, e) SSSR; thickness $h/b = 0.01, 0.1$.

4.2.2. Classical end conditions: Convergence study and comparative studies. Tables 1–4 show the first nine natural frequencies of square plates, with CCCC,

Table 1. Convergence studies of frequency parameter for CCCC plate.

$t = h/b = 0.001$	# of terms ($3 \times r^2$)	$\omega(1)$	$\omega(2)$	$\omega(3)$	$\omega(4)$	$\omega(5)$	$\omega(6)$	$\omega(7)$	$\omega(8)$	$\omega(9)$
	$r = 2$	36.1138	73.7476	73.7476	108.8614					
	$r = 3$	36.0128	73.5018	73.5018	108.8614	131.7855	132.3480	166.0481	166.0481	
	$r = 4$	36.0128	73.4715	73.4715	108.3894	131.7855	132.3480	165.4751	165.4751	210.7846
	$r = 5$	35.9978	73.4322	73.4322	108.3894	131.6567	132.2657	165.3188	165.3188	210.6410
Sources	LEISSA [12]	35.9920	73.4130	73.4130	108.2700	131.6400	132.2400			
	XIANG <i>et al.</i> [23]	35.9850	73.3963	73.3963	108.2202	131.5766	132.2181	165.1934	165.1944	211.7207
Deviation [%]	Present	0.0138	0.0258	0.0258	0.1014	0.0075	0.0151			

Table 2. Convergence studies of frequency parameter for SSSS plate.

$t = h/b = 0.001$	# of terms ($3 \times r^2$)	$\omega(1)$	$\omega(2)$	$\omega(3)$	$\omega(4)$	$\omega(5)$	$\omega(6)$	$\omega(7)$	$\omega(8)$	$\omega(9)$
	$r = 2$	19.74050	49.34970	49.34970	78.96120					
	$r = 3$	19.74050	49.34970	49.34970	78.96120	98.69670	98.69670	128.30950	128.30950	
	$r = 4$	19.74050	49.34970	49.34970	78.96120	98.69670	98.69670	128.30950	128.30950	167.78070
	$r = 5$	19.74050	49.34970	49.34970	78.96120	98.69670	98.69670	128.30950	128.30950	167.78070
Sources	LEISSA [12]	19.73920	49.34800	49.34800	78.95680	98.69600	98.69600	128.30490	128.30490	167.78330
	XIANG <i>et al.</i> [23]	19.73920	49.34400	49.34600	78.95280	98.69300	98.69300	128.29790	128.29890	167.77930
Deviation [%]	Present	0.00658	0.00344	0.00344	0.00557	0.00070	0.00070	0.00358	0.00358	0.00154

Table 3. Convergence studies of frequency parameter for SCSC plate.

$t = h/b = 0.001$	# of terms ($3 \times r^2$)	$\omega(1)$	$\omega(2)$	$\omega(3)$	$\omega(4)$	$\omega(5)$	$\omega(6)$	$\omega(7)$	$\omega(8)$	$\omega(9)$
	$r = 2$	29.0007	55.0523	69.3645	94.8669					
	$r = 3$	28.9611	54.7970	69.3646	94.8670	102.3503	129.1310	140.9830	154.9801	
	$r = 4$	28.9616	54.7973	69.3440	94.6592	102.3504	129.1311	140.4234	154.9802	170.5737
	$r = 5$	28.9583	54.7602	69.3445	94.6595	102.2567	129.1205	140.4235	154.8493	170.4201
Sources	LEISSA [12]	28.9509	54.7431	69.3270	94.5853	102.2162	129.0955	140.2045	154.7757	170.3465
Deviation [%]	Present	0.0255	0.0312	0.0252	0.0783	0.0396	0.0193	0.1559	0.0475	0.0431

Table 4. Convergence studies of frequency parameter for CCCS plate.

$t = h/b = 0.001$	# of terms ($3 \times r^2$)	$\omega(1)$	$\omega(2)$	$\omega(3)$	$\omega(4)$	$\omega(5)$	$\omega(6)$	$\omega(7)$	$\omega(8)$	$\omega(9)$
	$r = 2$	31.9086	63.6958	71.2252	101.4065					
	$r = 3$	31.8472	63.4110	71.1626	101.2268	116.5227	130.4862	152.9063	160.0196	
	$r = 4$	31.8434	63.4024	71.1146	100.9374	116.5103	130.4381	152.2219	159.8675	190.0170
	$r = 5$	31.8365	63.3596	71.1058	100.9101	116.4129	130.4033	152.1786	159.6507	189.8616
Sources	LEISSA [12]	31.8290	63.3470	71.0840	100.8300	116.4000	130.3700			
Deviation [%]	Present	0.0235	0.0198	0.0306	0.0793	0.0110	0.0255			

SSSS, SCSC, and CCCS boundary conditions. The thickness ratio used is 0.001. Considering an increasing number of participatory modes in either direction, the fundamental frequency of each plate is seen to converge to the corresponding Kirchhoff's plate frequency, as shown by LEISSA [12] and/or XIANG [23]. The %age deviations of the frequencies by the present with respect to LEISSA [12] have been tabulated. LEISSA has tabulated the first six frequencies, while XIANG [23] has tabulated the first nine of them. The deviation is the minimum for the SSSS plate because, the Timoshenko beam mode shape for a SS beam is a simple sinusoidal function with lower slopes and curvatures, compared to those of a CC beam, where the mode shapes contains both sinusoidal and hyperbolic terms. The next few frequencies are also seen to converge reasonable well, for the four plates. There are *three* kinds of frequencies, as seen in Tables 1–4.

The authors have used this classification as an innovative attempt to distinguish the frequencies.

- Type (a): *Single frequencies*, when the coefficient C_{ij} , has $i = j$. Here, $i =$ dominant beam mode shape index in the x -direction; $j =$ dominant beam mode shape index in the y -direction.
- Type (b): *Repeated frequencies* or *Identical twins*: when i is odd and j is even, or vice-versa. The frequencies are exactly equal, which stand for repeated roots of the eigenvalue problem. Their mode shapes occur in pairs, i.e. they are identical, only rotated in space by 90 degrees.
- Type (c): *Non-repeated frequencies* or *Fraternal twins*: when i and j are both odd, or both even. These frequencies are nearly equal to each other, but they are the conjugate roots of the eigenvalue problem. Their mode shapes are very different from each other. These frequencies occur when the contributing beam mode shape(s) and its (their) curvature(s) are *not* orthogonal to each other.

There are all the three kinds of frequencies for a CCCC plate. The SSSS plate has either single (type a) or repeated (type b) frequencies since its contributing beam mode shapes and their curvatures are orthogonal to each other. This weakens the cross-coupling terms in the potential energy. For a SCSC and CCCS plate, all the frequencies are *Single*, since their beam mode shapes in either direction are different from each other.

Figure 5 gives the first $3 \times 3 = 9$ mode shapes of a square CCCC plate, with the dominant C_{ij} . All the nine mode shapes are seen to exactly and accurately match with those produced both experimentally (Amplitude Fluctuation – Electron Speckle Pattern Interferometry, AF-ESPI) and by FEA as mentioned in [15]. The diagonal of the table contains the *single* (type a) frequencies, in which we find the chessboard-like deflection configuration and nodal patterns

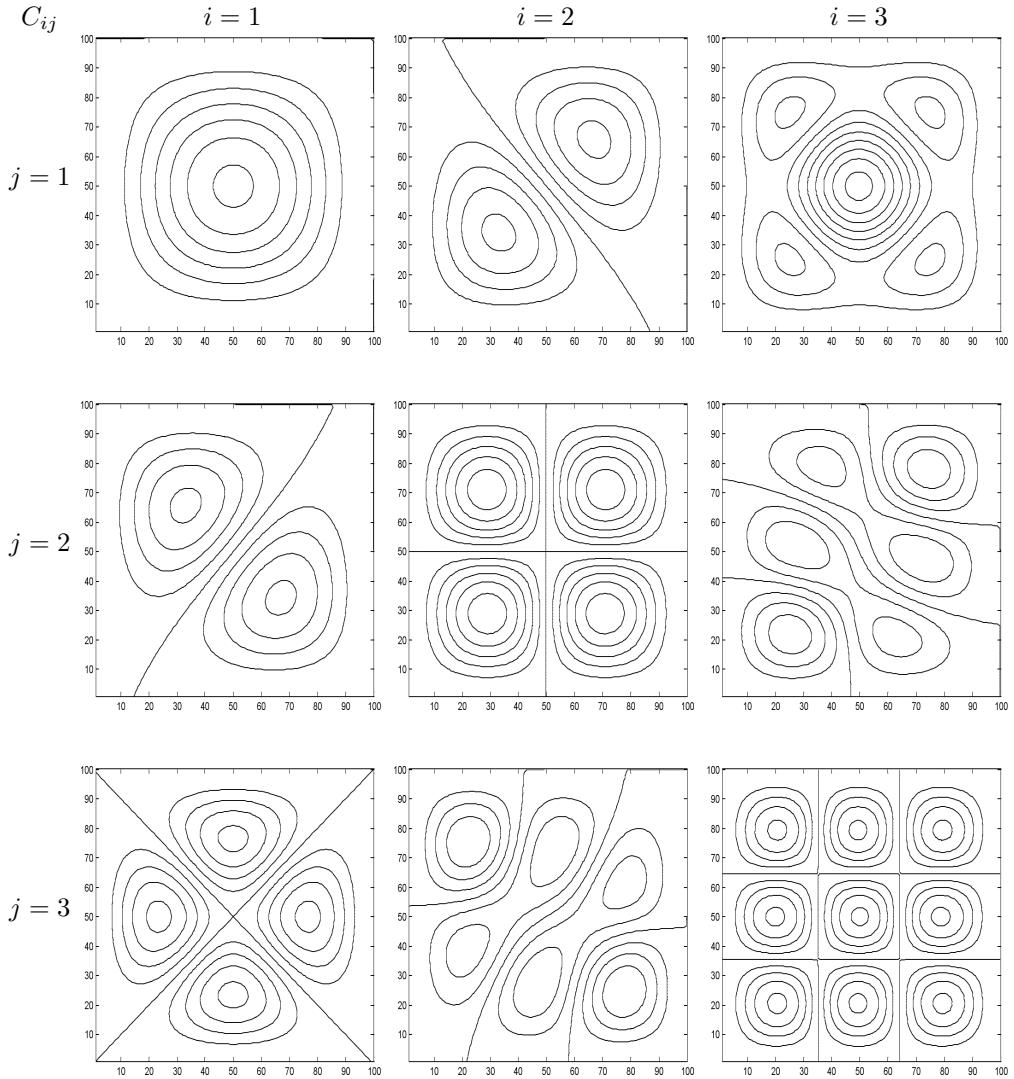


FIG. 5. First $3 \times 3 = 9$ mode shapes of a square CCCC plate, for slenderness ratio $h/b = 0.01$.

(nodal lines are parallel/perpendicular to the plate edges). The diagonals on either side of the main diagonal contain the *repeated* frequencies (type b) frequencies. The diagonals adjacent to them contain the *non-repeated* (type c) frequencies. The (type b) and (type c) frequencies appear alternately in the outer sub-diagonals. The first row gives the dominating Timoshenko beam mode shape in the x -direction, i.e. $i = 1, 2, \text{ or } 3$. The first column gives the dominating Timoshenko beam mode shape in the y -direction, i.e. $j = 1, 2, \text{ or } 3$. Each of the nine

mode shapes has been depicted based on the dominating C_{ij} , since the total Mindlin's plate mode shape is a weighted superposition of the product of the Timoshenko beam mode shapes in each direction.

Table 5 shows the eigenvectors C_{ij} , for the first nine natural frequencies of a CCCC plate, exactly corresponding to the respective mode shapes in Fig. 3. The eigenvectors have been listed as a matrix, with respect to the contributing Timoshenko beam mode shape index in either direction. In the fundamental mode shape, it is seen that the coefficient C_{11} dominates, and the rest of coefficients are much smaller. For a symmetric plate mode shape, the anti-symmetric beam mode shape, in either direction, hardly have any contribution. Similarly, for an anti-symmetric plate mode shape, the symmetric beam mode shapes, in either direction, hardly have any contribution. This is clearly seen from the first eigenvector, where, in order to generate the first Mindlin's plate mode shape, C_{11} (dominant), C_{13} , C_{31} (very mild, equal presence), C_{33} (trace), have contributions, but coefficients with any even subscript are absent.

Table 5. Eigenvector matrix of first $3 \times 3 = 9$ mode shapes of a CCCC plate.

	$i = 1$			$i = 2$			$i = 3$		
$j = 1$	1st mode shape (36.036)			2nd/3rd mode shape (73.498)			5th mode shape (131.621)		
	-1.0000	-0.0000	-0.0138	0.0000	-1.0000	-0.0000	-0.0000	-0.0000	-1.0000
	-0.0000	-0.0000	-0.0000	0.8680	-0.0000	0.0351	0.0000	0.0000	0.0000
	-0.0138	-0.0000	0.0029	0.0000	-0.0404	-0.0000	1.0000	-0.0000	0.0000
$j = 2$	2nd/3rd mode shape (73.498)			4th mode shape (108.752)			7th/8th mode shape (165.694)		
	-0.0000	0.8865	0.0000	-0.0000	-0.0000	0.0000	0.0000	-0.0234	-0.0000
	1.0000	0.0000	0.0404	-0.0000	-1.0000	0.0000	0.0396	-0.0000	-1.0000
	0.0000	0.0358	0.0000	0.0000	0.0000	-0.0000	0.0000	0.5892	0.0000
$j = 3$	6th mode shape (132.192)			7th/8th mode shape (165.694)			9th mode shape (210.241)		
	0.0266	-0.0000	-1.0000	0.0000	0.0396	0.0000	-0.0045	0.0000	0.0606
	-0.0000	-0.0000	-0.0000	0.0186	-0.0000	-0.4687	0.0000	-0.0000	-0.0000
	-1.0000	-0.0000	-0.1236	-0.0000	-1.0000	0.0000	0.0606	-0.0000	-1.0000

For the *single* (type a) frequencies, only one element of the diagonal of the eigenvector matrix dominates. The 4th mode shape in box (2, 2) of Table 5, for the *single* frequency, with the dominating C_{22} , has no contribution from any other mode shape, since their subscripts have odd digit(s). The 9th mode shape in box (3, 3) in Table 5, which is *single* (type a) frequency, has the largest

contribution from C_{33} , and mild ones from C_{13} and C_{31} , with a trace of C_{11} . The contributions from coefficients with at least one even subscript will not occur here.

For the *identical twins* (type b) frequencies, eigenvectors are repeated, just like the eigenvalues are. The second and third mode shapes have *repeated* frequencies, with similar eigenvectors. A closer look at box (1, 2) and box (2, 1) of Table 5 shows that C_{12} and C_{21} dominate respectively, with the C_{21} and C_{12} a close second in prominence, again respectively. Both these identical twins have traces of C_{23} and C_{32} . But they have absolutely no contribution from those coefficients whose both subscripts are odd, or both are even.

This is once again seen in the 7th and the 8th mode shapes, which have *repeated* frequencies, and similar eigenvectors. In Table 5, box (2, 3) and (3, 2) have C_{23} and C_{32} dominating, respectively. The second largest contribution comes from the counterpart C_{32} and C_{23} , respectively. Traces of C_{12} and C_{21} are present in both. But again, there are no contributions from those coefficients with both subscripts even, or both odd. However, for the *fraternal twins* (type c) frequencies, eigenvectors are starkly different from each other. The eigenvectors have two equally dominating elements creating the mode shapes.

As seen in Table 5, the 5th and 6th frequencies are fraternal twins, where C_{13} and C_{31} are equally in prominence. Observing box (1, 3) and box (3, 1) in Table 5, it is seen that there is no contribution from any coefficient with at least one even subscript, i.e. C_{12} , C_{21} , C_{22} , C_{23} , C_{32} have no contribution. However, it is surprising to find that for the '*junior*' fraternal twin (5th mode shape, frequency = 131.621), there is no contribution from C_{11} and C_{33} , leading to a slightly lower frequency than the '*senior*' fraternal twin (6th mode shape, frequency = 132.192). Contributions from C_{13} and C_{31} increase the potential energy of the '*senior*' fraternal twin', leading to a higher natural frequency. The details may be found in [4]. This is an improved and more specific classification from those depicted in [3].

Figure 6 shows the first $3 \times 3 = 9$ mode shapes of the square CCSS plate with the dominant C_{ij} , while Table 6 shows their eigenvectors. Observing the fundamental mode shape, it is clear that the top and right edges are clamped (C) while the left and bottom edges are hinged (S). The deflection contours are closer to the hinged edge, since the slopes are larger there. The *single* frequencies in the diagonal of Fig. 6 show a similar trend. In box (2, 1), and box (3, 2), the nodal line is exactly along the diagonal because there is a C and a S side each on its either side. However, for the '*identical twin*' in box (1, 2) and box (2, 3) respectively, it is away from the diagonal and intersects the two S edges.

The eigenvectors of *identical twins*, in the matrix form, are symmetric. But they have different frequencies due to different diagonal elements of the eigenvec-

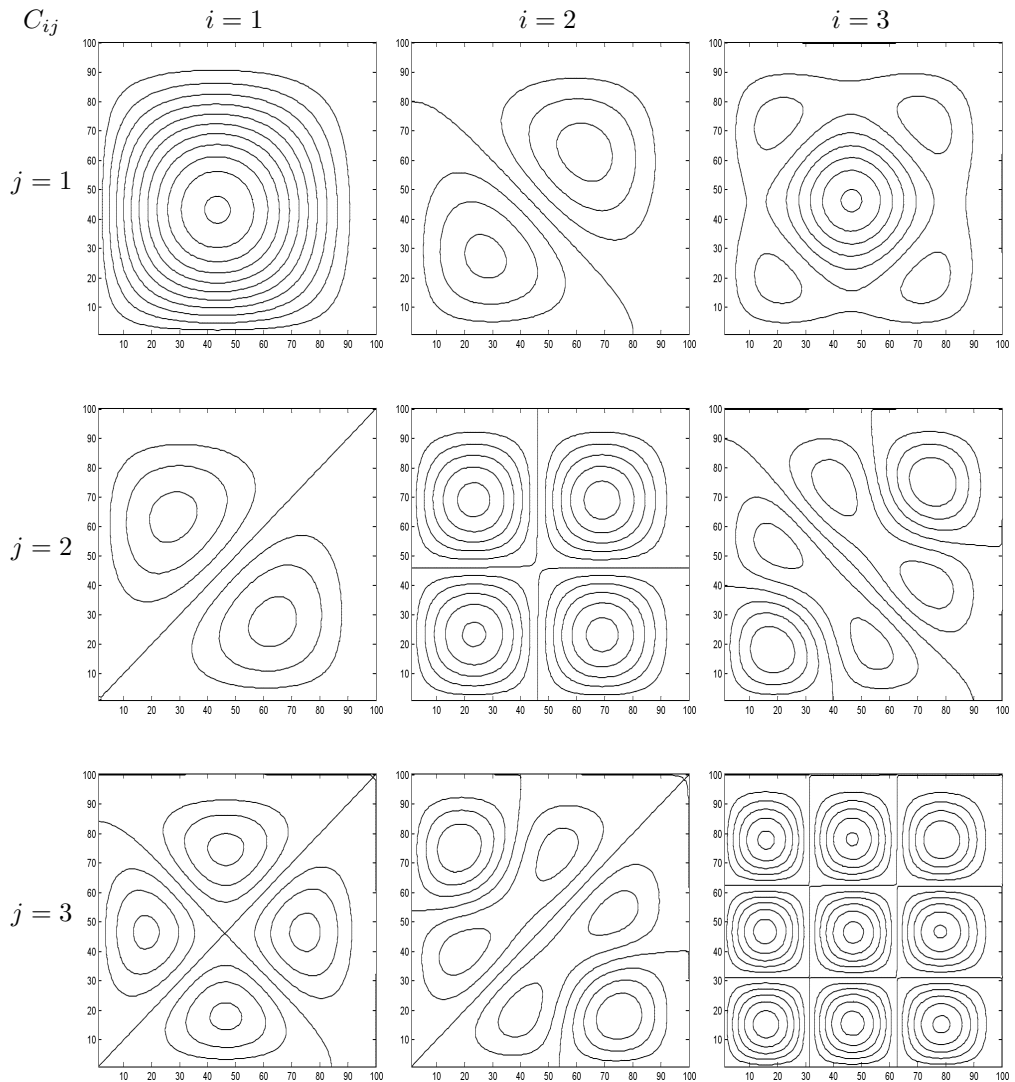


FIG. 6. First $3 \times 3 = 9$ mode shapes of a square CCSS plate, for slenderness ratio $h/b = 0.01$.

tors; e.g., box (1, 2) and box (2, 1) have equal non-diagonal terms, but the one with bigger diagonal term has a higher frequency. The ‘*fraternal twins*’ have very different but symmetric/skew-symmetric eigenvectors. All ‘twins’ have at least two elements equally strong. From the frequencies, it may seem that box (1, 2) and box (1, 3) are also twins since their frequencies are close. However, whether two frequencies are twins or not are decided by the symmetry/skew-symmetry of the matrix-form of eigenvectors.

Table 6. Eigenvector matrix of first $3 \times 3 = 9$ mode shapes of a CCSS plate.

	$i = 1$			$i = 2$			$i = 3$		
$j = 1$	1st mode shape (27.0599)			2nd/3rd mode shape (60.5598)			5th/6th mode shape (114.5983)		
	1.000	-0.032	0.006	-0.000	1.000	0.019	-0.0120	0.0172	1.000
	-0.032	-0.001	0.001	-0.999	0.000	0.021	0.0172	0.0047	-0.100
	0.006	0.001	-0.000	-0.019	-0.021	-0.000	0.9990	-0.1000	0.065
$j = 2$	2nd/3rd mode shape (60.8059)			4th mode shape (92.9065)			7th/8th mode shape (146.2177)		
	0.064	0.999	-0.014	-0.007	-0.077	0.008	0.0040	0.0107	-0.105
	1.000	-0.153	0.020	-0.077	-1.000	0.049	0.0100	-0.1030	-1.000
	-0.014	0.020	0.001	0.008	0.049	-0.000	-0.1050	-0.9990	0.156
$j = 3$	5th/6th mode shape (114.7405)			7th/8th mode shape (145.9376)			9th mode shape (188.5305)		
	0.000	-0.017	-1.000	-0.000	0.023	0.106	0.0006	-0.0020	-0.024
	0.017	0.000	0.107	-0.023	-0.000	1.000	-0.0020	0.0070	0.080
	0.999	-0.107	0.000	-0.106	-0.999	0.000	-0.0240	0.0800	1.000

Figure 7 shows the first $3 \times 3 = 9$ mode shapes of the square SCSC plate. Here, all the plate mode shapes have the chessboard configuration, i.e. the nodal lines are either parallel or perpendicular to the edges of the plate. The eigenvectors of each mode shape has only one dominant participatory element, while the second strongest participation is merely 2% of even less than the strongest. Square plates with CCSS and SSSC edge configurations generate similar mode shapes. All these plates have distinct frequencies, with no *twins*, whether *identical* or *fraternal*. All the six plates have their mode shapes verified with respect to those obtained through the Classical plate theory.

4.3. Rectangular plate vibration

Apart from the various boundary conditions and slenderness ratios, the third parameter explored in this study is the *aspect ratio* of the Mindlin’s plate. This parameter has a strong influence on the plate natural frequencies, and its mode shapes. The eigenvalues and eigenvectors from the eigenvalue problem in Eq. (3.18) get altered according to the aspect ratio, slowly approaching the behaviour of a Timoshenko beam, for aspect ratios close to 0.1. The plate natural frequencies for the classical boundary conditions, namely, SSSS, SSSC, SCSC, SSCC, SCCC, and CCCC have been verified with LEISSA [12].

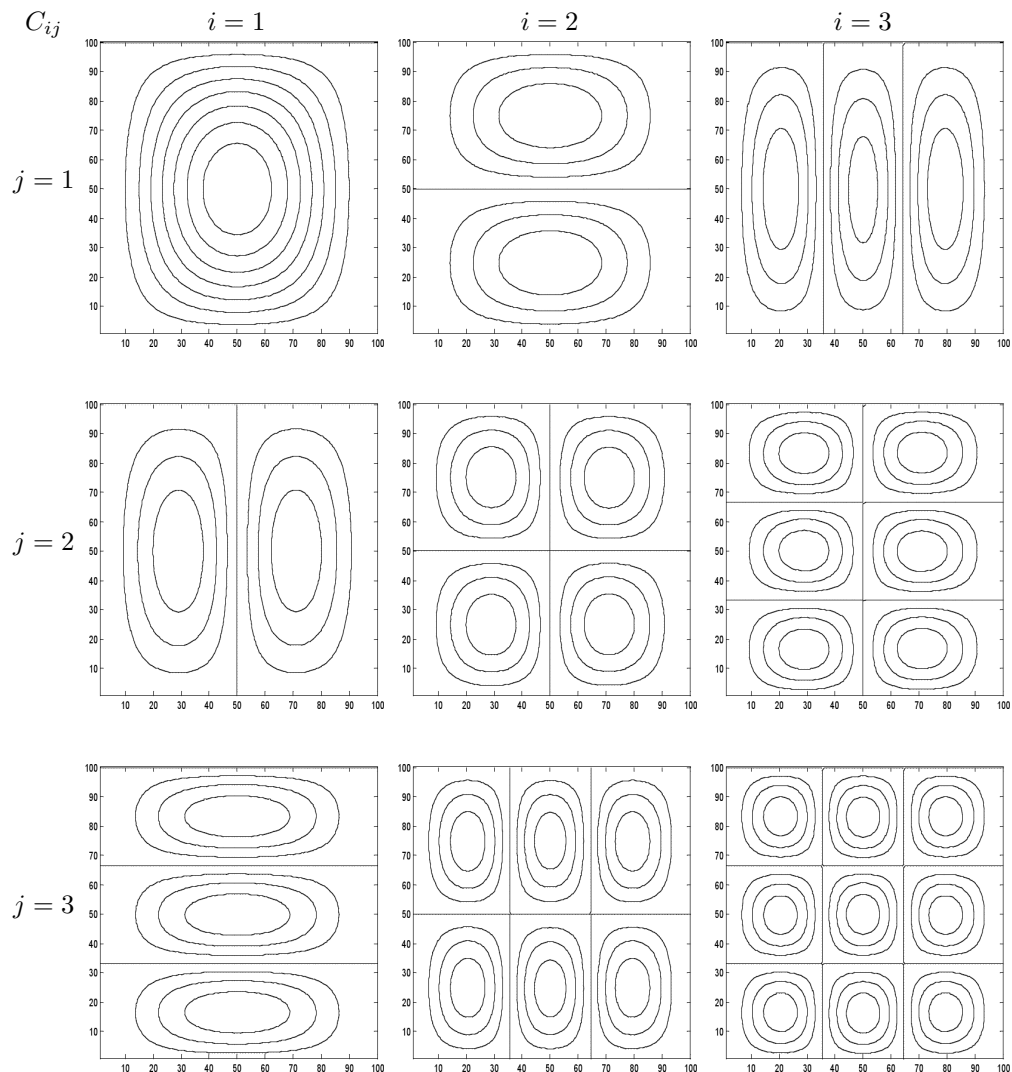


FIG. 7. First $3 \times 3 = 9$ mode shapes of a SCSC plate, for slenderness ratio $h/b = 0.01$.

4.3.1. Classical edge conditions: convergence and comparative studies. Tables 7 and 8 show the convergence of the first six natural frequencies of rectangular plates, with classical boundary conditions; with an aspect ratio of $a/b = 1.5$ and 0.6 respectively. The Mindlin's plate frequencies from the present method are compared with those of the Kirchhoff's plate by LEISSA [12], who provides the first six frequencies (by Ritz method); and also with the Kirchhoff's plate frequencies by LIEW *et al.* [14], who provide only the first four of them (by Rayleigh-Ritz method). In the present study, the Mindlin's plate analysis converges to the

Table 7. Convergence studies of frequency parameter for Mindlin’s plates with 6 different boundary conditions, for aspect ratio $a/b = 1.5$, $t = h/b = 0.001$.

Plates	Sources	$\omega(1)$	$\omega(2)$	$\omega(3)$	$\omega(4)$	$\omega(5)$	$\omega(6)$
CCCC	Present	60.782	93.9014	148.850	149.766	179.864	226.995
	LEISSA [12]	60.772	93.860	148.82	149.74	179.66	226.92
	LIEW <i>et al.</i> [14]	60.77	93.87	148.83	149.88		
SSSS	Present	32.0780	61.6887	98.6977	111.0370	128.3111	177.6627
	LEISSA [12]	32.0762	61.6850	98.6960	111.0330	128.3049	177.6529
	LIEW <i>et al.</i> [14]	32.08	61.71	98.76	111.57		
CCSS	Present	44.9006	76.5748	122.3622	129.4444	152.6550	202.7058
	LEISSA [12]	44.893	76.554	122.33	129.41	152.58	202.66
	LIEW <i>et al.</i> [14]	44.89	76.58	122.47	129.74		
SCSC	Present	56.3631	79.0043	123.2106	146.2977	170.1731	189.1925
	LEISSA [12]	56.3481	78.9836	123.1719	146.2677	170.1112	189.1219
	LIEW <i>et al.</i> [14]	56.35	79.01	123.28	146.31		
SCSS	Present	42.5751	69.0693	116.3503	121.1265	147.8101	184.2050
	LEISSA [12]	42.5278	69.0031	116.2671	120.9956	147.6353	184.1006
	CCCCS	Present	48.2592	85.5897	124.0448	144.0477	158.5559
	LEISSA [12]	48.167	85.507	123.99	143.99	158.36	214.78

Table 8. Convergence studies of frequency parameter for Mindlin’s plates with 6 different boundary conditions, for aspect ratio $a/b = 0.6$, $t = h/b = 0.001$.

Plates	Sources	$\omega(1)$	$\omega(2)$	$\omega(3)$	$\omega(4)$	$\omega(5)$	$\omega(6)$
CCCC	Present	27.0257	41.749	66.193	66.636	79.940	100.966
	LEISSA [12]	27.010	41.716	66.143	66.552	79.850	100.85
	LIEW <i>et al.</i> [14]	27.01	41.73	66.16	66.66		
SSSS	Present	14.2573	27.4187	43.8656	49.3531	57.0282	78.9637
	LEISSA [12]	14.2561	27.4156	43.8649	49.3480	57.0244	78.9568
	LIEW <i>et al.</i> [14]	14.26	27.44	43.90	49.63		
CCSS	Present	19.9562	34.0350	54.3828	57.53453	67.8474	90.0972
	LEISSA [12]	19.952	34.024	54.370	57.517	67.815	90.069
	LIEW <i>et al.</i> [14]	19.95	34.06	54.43	57.48		
SCSC	Present	17.3786	35.3629	45.4481	62.0773	62.4129	88.9083
	LEISSA [12]	17.3730	35.3445	45.4294	62.0544	62.3131	88.8047
	LIEW <i>et al.</i> [14]	17.38	35.37	45.62	62.20		
SCSS	Present	15.5928	31.1120	44.5880	55.4600	59.5422	83.7464
	LEISSA [12]	15.5783	31.0724	44.5644	55.3926	59.4627	83.6060
	CCCCS	Present	25.8695	38.1147	60.3402	65.5337	77.6054
	LEISSA [12]	25.861	38.102	60.325	65.516	77.563	92.154

Kirchhoff's plate frequencies, since the thickness ratio is as low as $h/b = 0.001$, for which the shear deformation and rotary inertia become negligible.

4.3.2. *Rectangular plate: asymptotic behaviour extreme aspect ratio.* Figure 8 shows the asymptotic behaviour of the plate natural frequencies, for two thickness ratios, with respect to the aspect ratio of the plate. The CCCC/SSSS plate frequency is seen to approach to the corresponding CC/SS beam frequency for an aspect ratio of 0.1, 10. In these plots, for the $A_s > 1$, the frequency has been non-dimensionalized further by $1/A_s^2$. For $A_s < 1$, the plate non-dimensional parameters for the beam and the plate are consistent. Similarly, SCSC plate behaves like a CC beam for $A_s \sim 10$, and like a SS beam for $A_s \sim 0.1$. The SSCC square plate frequency descends to the SC beam frequency for both the extreme aspect ratios. The beam mode shapes in the shorter direction hardly contribute in generating the plate mode shape, and hence the natural frequency.

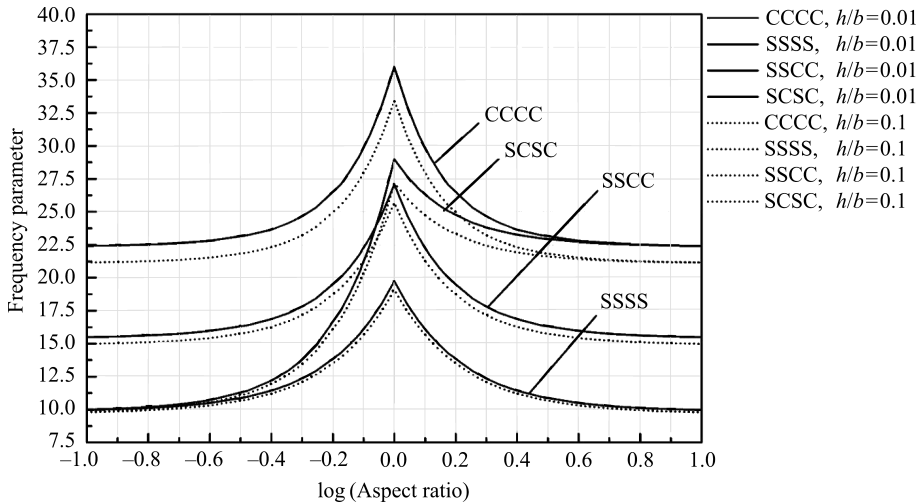


FIG. 8. Natural frequency of plates (CCCC, SCSC, SSCC, SSSS) with respect to aspect ratio $0.1 < A_s < 10$.

5. DISCUSSION

The free vibration of the plate is analysed by the RRM. This requires the pre-generation of the admissible or trial functions, which are the Timoshenko beam mode shapes in either direction. The beam mode shape, and the pure-bending slope mode shape, are functions of the boundary conditions only, which are influenced by the torsional spring constant. The product of the two Timoshenko beam mode shapes (i in number in the x -direction and j in number in the

y -direction) gives the $(i-j)$ -th ‘plate trial function’. Each ‘plate trial function’ has its own contribution to the final plate mode shape. The assumed plate mode shape, with unknown coefficients, is used to minimize the natural frequency. The potential energy of the plate due to its curvature and shear deformation is augmented by the torsional springs at the edges. The pure-bending slopes of the plate, in both directions, are also required in the estimation of the potential energy. The kinetic energy is augmented by the rotary inertia. The torsional springs do not participate in the kinetic energy of the vibration. This sets up an eigenvalue problem, whose eigenvalues are the squares of the natural frequencies; and the eigenvectors give the unknown coefficients, leading to the final plate mode shape.

This study has considered the edges to be specially restrained against rotation. The deflection is zero at all the edges; however, the bending moment at the end is a fraction of the bending moment for the clamped (classical edge) boundary condition. The modelling of the special boundary condition as a torsional spring, uniformly distributed along all the edges, allows the continuous changing of the spring constant [$\text{N} \cdot \text{m}/\text{rad}$], in order to generate the plate natural frequencies for a wide range of edge constraints, from the classical negative extreme of simply-supported condition to the classical positive extreme of the clamped (built-in) condition. All the six classical conditions of the combinations and permutations of clamped and simply-supported edges have been generated and their natural frequencies have been verified with the existing literature, for two different thickness ratios ($h/b = 0.01, 0.1$).

The *transition zone* of the natural vibration, i.e. the spring constant at which the plate switches from the ‘simply-supported’ to the ‘clamped’ behaviour, has been established and verified for various edge conditions, two thicknesses, and three different aspect ratios. The transition zone is seen to be independent of the aspect ratios: it is seen to occur between $1 < K_R < 1000$, for three different aspect ratios, i.e. $a/b = 0.4, 1.0, 1.5$. At a thickness ratio $h/b = 0.001$, the Mindlin’s plate analysis is seen to converge back to the Kirchhoff’s plate frequencies. This is verified for all six classical plates and four different aspect ratios.

The CCCC square plate is seen to produce *three different kinds of natural frequencies*; and their corresponding mode shapes have also been categorized and verified with literature. Each eigenvector, of the first 9 mode shapes of the CCCC plate has been scrutinized to provide insights into their repeating and non-repeating frequencies, named as the ‘identical twins’ and the ‘fraternal twins’. The identical twins have exactly the same frequency, and their mode shapes are mirror images of each other. The fraternal twins have very close but different frequencies, but their mode shapes are very different from each other. Interestingly, the SSSS plate does not have the fraternal twins among its frequencies, since the cross-coupling between the beam-wise curvatures along

the two perpendicular directions are absent (since the SS beam mode shape and its curvature are orthogonal to each other). Both these plates also have the ‘single’ frequencies (type a), where the same Timoshenko mode shape from either direction participate strongly in generating the plate mode shape. The SSCC plate also produces ‘repeated’ frequencies (type b) or ‘identical’ twins. The other three classical plates (and their special counterparts) have only the ‘single’ frequencies. An *asymptotic study* of the Mindlin’s plate natural frequency with respect to the aspect ratio, has also been presented. For $a/b > 10$, or $a/b < 0.1$, the plate begins to behave like the corresponding beam. This study gives insights into the participation of the Timoshenko beam mode shapes in either direction, with respect to the aspect ratio. As the aspect ratio becomes non-unity, the beam-wise participation in the plate mode shape becomes more prominent from the longer side.

6. CONCLUSIONS

Thus, the following distinct conclusions can be arrived at from this work:

- *Timoshenko beam* mode shapes, derived from the free vibration analysis of the beam, can be used as superior closed-form trial functions in the Mindlin’s plate vibration analysis. They encompass the potential energy of the beam including the special edge conditions.
- *Rotationally constrained edges*: The use of the dummy rotational spring constants in Eq. (3.16) eliminates the need for translational springs in order to indirectly achieve the plate boundary conditions. The lateral strain of the plate at each edge is taken care of by the dummy variables, compensating for the approximation in the plate boundary conditions.
- *Transition zone*: The edge constraint with $K_R < 1$, behaves like a simply-supported edge, while an edge with $K_R > 10^4$ behaves like a clamped edge.
- *Eigenvectors*: The plate mode shapes are highly sensitive to the accuracy of the eigenvectors. The dominant cross-coupled participation of the beam-wise Timoshenko functions in either direction leads to the distinct classification of the natural frequencies and plate mode shapes.
- *Aspect ratio*: plates, where one side is at least ten times longer than the other side, may be safely analysed by the closed-form Timoshenko beam theory.

The **relevance of this work** is seen in several distinct ways:

- The modelling of the special edges need *not* require translational springs in order to capture the boundary conditions of the specific plates studied in this work.

- The range of the torsional spring constant for which the plate may be safely assumed to behave like a classical edge plate is demarcated. Working with classical end conditions is easier, and the clear demarcation of *transition zone* helps the structural designer avoid the more cumbersome special edge condition analysis.
- For a *slenderness* ratio $h/b = 0.001$, Kirchhoff's plate theory is sufficient for at least the first nine natural frequencies. For $h/b = 0.01$, the shear deformation and rotary inertia begin to become prominent, especially at the higher-order modes.
- Theoretical generation of the plate mode shapes requires a very accurate eigenvector, without which the comparison with experimentally obtained mode shapes (cymatics) is not possible. Observation of plate mode shape indicates the corresponding natural frequency as a corollary.
- *Modeshape patterns* clearly indicate the nodal lines, and thus, the stress distribution pattern in a dynamic system.
- From the *asymptotic study* of the plate natural frequencies with respect to the aspect ratio, the structural designer knows the aspect ratio at which s/he can safely perform beam analysis of a plate.

REFERENCES

1. BAPAT A.V., VENKATRAMANI N., SURYANARAYAN S., *Simulation of classical edge conditions by finite elastic restraints in the vibration analysis of plates*, Journal of Sound and Vibration, **120**(1): 127–140, 1988.
2. CHUNG J.H., CHUNG T.Y., KIM K.C., *Vibration analysis of orthotropic Mindlin Plates with edges elastically restrained against rotation*, Journal of Sound and Vibration, **163**(1): 151–163, 1993.
3. COURANT R., HILBERT D., *Methods of mathematical physics*, Vol. I, 1st English Ed., Interscience Publishers, Inc., New York, 1966.
4. DATTA N., VERMA Y., *Accurate eigenvector-based generation and computational insights of Mindlin's plate mode shapes for twin frequencies*, International Journal of Mechanical Sciences, **123**: 64–73, 2017.
5. DAWE D.L., ROUFAEIL O.L., *Rayleigh-Ritz vibration analysis of Mindlin plates*, Journal of Sound and Vibration, **69**(3): 345–359, 1980.
6. DE ROSA M.A., LIPPIELLO M., *Natural vibration frequencies of tapered beams engineering*, Engineering Transactions, **57**(1):45–66, 2009.
7. GORMAN D.J., *A comprehensive study of the free vibration of rectangular plates resting on symmetrically distributed uniform elastic edge supports*, ASME Journal of Applied Mechanics, **56**(4): 893–899, 1989.
8. GORMAN D.J., *A general solution for the free vibration of rectangular plates resting on uniform elastic edge supports*, Journal of Sound and Vibration, **139**(2): 325–335, 1990.

9. HUANG T.C., *The effect of rotary inertia and of shear deformation on the frequency and normal mode equations of uniform beams with simple end conditions*, Journal of Applied Mechanics, **28**(4): 579–584, 1961.
10. LAURA P.A.A., GROSSI R.O., *Transverse vibration of a rectangular plate elastically restrained against rotation along three edges and free on the fourth edge*, Journal of Sound and Vibration, **59**(3): 355–368, 1978.
11. LAURA P.A.A., ROMANELLI E., *Vibrations of rectangular plates elastically restrained against rotation along all edges and subjected to a biaxial state of stress*, Journal of Sound and vibration, **37**(3): 367–377, 1974.
12. LEISSA A.W., *The free vibration of rectangular plates*, Journal of Sound and Vibration, **31**(3): 257–293, 1973.
13. LEISSA A.W., *Vibration of plates*, NASA SP–160, 1969.
14. LIEW K.M., LAM K.Y., CHOW S.T., *Free vibration analysis of rectangular plates using orthogonal plate function*, Computers and Structures, **34**(1): 79–85, 1990.
15. MA C.C., HUNAG C.H., *Experimental whole-field interferometry for transverse vibration of plates*, Journal of Sound and Vibration, **271**(3–5): 493–506, 2004.
16. MAGRAB E.B., *Natural frequencies of elastically supported orthotropic rectangular plates*, Journal of Acoustical Society of America, **61**(1): 79–83, 1977.
17. MINDLIN R.D., *Influence of rotary inertia and shear on flexural motions of isotropic, elastic plates*, Transactions of the American Society of Mechanical Engineers, Journal of Applied Mechanics, **18**(1): 31–38, 1951.
18. MINDLIN R.D., SCHACKNOW A., DERESIEWICZ H., *Flexural vibrations of rectangular plates*, Transactions of the American Society of Mechanical Engineers, Journal of Applied Mechanics, **23**(3): 430–436, 1956.
19. SAHA K.N., KAR R.C., DATTA P.K., *Free vibration analysis of rectangular Mindlin plates with elastic restraints uniformly distributed along the edges*, Journal of Sound and Vibration, **192**(4): 885–904, 1996.
20. TIMOSHENKO S.P., *Vibration problems in engineering*, 3rd ed., D. Van Nostrand Company, Inc., New York., pp. 329–331, 1955.
21. TRAILL-NASH R.W., COLLAR A.R., *The effects of shear flexibility and rotatory inertia on the bending vibrations of beams*, Quarterly Journal of Mechanics and Applied Mathematics, **6**(2): 186–222, 1953.
22. WARBURTON G.B., EDNEY S.L., *Vibrations of rectangular plates with elastically restrained edges*, Journal of Sound and Vibration, **95**(4): 537–552, 1984.
23. XIANG Y., LIEW K.M., KITIPORNCHAI S., *Vibration analysis of rectangular Mindlin plates resting on elastic edge supports*, Journal of Sound and Vibration, **204**(1): 1–16, 1997.
24. ZHOU D., *Vibrations of Mindlin rectangular plates with elastically restrained edges using static Timoshenko beam functions with the Rayleigh-Ritz method*, International Journal of Solids and Structures, **38**(32–33): 5565–5580, 2001.

Received July 26, 2017; accepted version February 8, 2018.
